Supporting Information

Deep reconstruction of Ni-Al-based pre-catalysts for highly efficient and durable anion-exchange membrane (AEM) electrolyzer

Tao Jiang [a, b] *, Xinge Jiang [c], Vasileios Kyriakou [a], Karel Bouzek [d], Hanlin Liao [c]

[a] *Department of Chemical Engineering, Engineering and Technology Institute Groningen (ENTEG), University of Groningen, Nijenborgh 4, 9747 AG, Groningen, The Netherlands*

[b] *Institute of Technical Thermodynamics, German Aerospace Center (DLR), Stuttgart 70569, Germany*

[c] *UBFC, ICB-PMDM-LERMPS UMR6303, Sevenans 90010, France*

[d] *Department of Inorganic Technology, University of Chemistry and Technology Prague, 166 28 Prague 6, Czech Republic*

AUTHOR INFORMATION

Corresponding Author
*E-mail: taojiang0510@gmail.com

Experimental section

Materials and chemicals

Nickel plate (NP, 99.8 %, Pingding City Lushan Yaxing Carbon Material Co., Ltd., China); Ni foam (NF, ≥99.8%, XIAMEN TOB NEW ENERGY TECHNOLOGY CO., LTD, China); NiAl (56/44) powder (H.C.Starck, Germany); KOH (99.5%, Sigma-Aldrich®); KNa tartrate-tetrahydrate (Sigma-Aldrich®); IrO_2 (99.9% trace metals basis; Alfa Aesar); Nafion (Alfa Aesar); 5cm^2 AEM cell hardware (Dioxide materials); Sustainion® X37-50 Grade RT Membrane (Dioxide materials).

Preparation of the HNA-CA pre-catalysts.

Firstly, the NiAl feedstock powder was used to deposit Ni–Al alloy coatings on NP. The NPs ($35\times35\times0.5$ mm^3) with holes of 1 mm aperture evenly distributed were ultrasonically cleaned by acetone, deionized water, and absolute ethyl alcohol in sequence for 25 min, and then dried in the air for 30 min. Then the Ni-Al alloy coatings (HNA) with a thickness of ca. 100 μm were obtained by High-velocity oxy-fuel (HVOF) spray (JP-5000 HVOF) with a certain spraying parameter (Table S1). In a subsequent chemical dealloying activation process, the as-obtained HNA precursors were chemically activated in 6 M KOH (contained 10 wt.% KNa tartrate-tetrahydrate) at 80 °C for 24 h to form HNA-CA. To avoid precipitation of aluminium hydroxide in the mesopores/microchannels of the obtained sponge-like structure, the solution contained 10 wt.% KNa tartrate-tetrahydrate (Rochelle salt) as a complexing agent. The resulting HNA-CA samples are easily oxidized because of extremely high activity, so they must be kept under 6 M KOH solution after activation.

Preparation of HNA-CA-H and HNA-CA-O electrodes

Electrochemical activation (ECA) of the HNA-CA ($35\times30\times0.5$ mm^3) pre-catalysts was simply implemented by employing HNA-CA as both cathode and anode under 800 mA cm^{-2} (6 M KOH at 80 °C) driven by a power supply (VOLTCRAFT DSP-6010) for 2 hours. The resulting cathode and anode were identified as HNA-CA-H and HNA-CA-O, respectively, which would be evaluated in a three-electrode-test system and employed in a 5 cm^2 AEM cell.

Fabrication of IrO_2/NF electrodes

To prepare the IrO_2/NF electrodes, 100 mg IrO_2 (Alfa Aesar), 200 μL Nafion (Alfa Aesar), 1 mL ethanol, and 1 mL deionized water were ultrasonicated for 60 min to obtain a homogeneous dispersion. Then, a piece of clean NF ($30\times30\times1$ mm^3) was dipped into the dispersion, which was then dried in air at 60 °C for 6 h. The mass loading of the IrO_2 catalyst on nickel foam was controlled to be ca. 4 mg cm^{-2}.

Materials characterization

XRD was performed with Bruker AXS D8 focus, equipped with a cobalt anticathode ($\lambda = 1.78897$ Å), and operated at 35 kV, 40 mA. SEM was carried out using a JEOL-JSM-7800F system equipped with an EDS analysis system (BRUCKER SDDX-Flash 6130; Zeiss Gemini Ultra plus microscope). The contact angle measurement was carried out by dropping 6 μL deionized water on the electrode surface with a dosing rate of 1 μL s^{-1} (DataPhysics Optical Contact Angle System OCA 15EC) and the data were analyzed with the SCA20 software. The measurements were conducted more than 3 times per sample to increase the accuracy of the data. UHV-XPS analysis has been performed using a Thermo Scientific ESCALAB 250 ultra-high vacuum (UHV) facility operated at a pressure of 1×10^{-9} mbar. As an X-ray source (Thermo XR4) the Al Kα line was used. The detection spot in the sample covered an area of 0.8 mm^2. The depth profiles were determined by high energy Ar$^+$-sputtering using a Thermo

EX05 ion gun at the flowing sputtering conditions: $2-3 \times 10^{-8}$ mbar at partial pressure, $3-7$ μA Ar$^+$ current at a sample area of 3×4 mm^2, 2 kV acceleration voltage, and 10 mA emission current. Transmission electron microscopy (TEM) measurements were done using an FEI Tecnai G^2 F20 S-TWIN TEM operated at 200 kV in the TEM/STEM mode. Samples were prepared by ultrasonic dispersion in ethanol and then a droplet of the dispersion was allowed to dry on a holey-carbon-coated copper grid. Bright-field and high-angle annular dark-field (HAADF) images were recorded. Distilled water and ethanol were used to thoroughly clean all the samples before testing commenced.

Electrochemical half-cell measurements (three-electrode test system)

All electrochemical measurements were carried out using an Autolab 128N Electrochemical Workstation with a developed in-house three-electrode test bench. Hydrogen Reference Electrode HydroFlex (Gaskatel GmbH, Germany) was used as the reference electrode. The potential measured using this Hydrogen Reference Electrode (HRE) as the reference electrode didn't require any complex conversion to Reversible Hydrogen Electrode (RHE), allowing any tested temperature and pH of the electrolyte, namely $E_{RHE} = E_{HRE}$. Furthermore, HRE is suitable for the full pH range from -2 to 16 and a temperature range from -30 °C to 200 °C. A nickel plate (10 mm×10 mm×0.5 mm) was used as the counter electrode (CE). HNA-CA-H was used directly as the working electrode in the HER test with bare NP, HNA-CA, and Pt foil as control samples. HNA-CA-O was used directly as the working electrode in the OER test with bare NP, HNA-CA, and IrO$_2$/NF as control samples. To better illustrate the catalytic activity of the materials, we tested all the samples under 1 M KOH at room temperature. This study's current density values of LSV curves refer to the geometric surface area. 1 M KOH solutions were saturated with O$_2$ before OER tests at room temperature. Linear sweep voltammetry (LSV) curves were recorded at a scan rate of 3 mV s^{-1}, and each measurement was repeated at least three times to avoid any incidental error. Tafel slopes were derived from LSV obtained by plotting overpotential against log (j, current density) after iR correction ($E_{iR}=E - j \times R_s$) in all the above test conditions. The electrochemical impedance spectroscopy (EIS) measurement was conducted in the frequency range of 100 kHz to 0.1 Hz with an amplitude of 5 mV under a fixed bias of -0.3 V vs. RHE ($\eta = 300$ mV) for HER, and 1.53 V vs. RHE ($\eta = 300$ mV) for OER.

The ECSA was determined by measuring the capacitive current associated with double-layer charging from the scan-rate dependence of CVs. For this, the potential window for CVs was 0.2 – 0.4 V vs. RHE for HER. The scan rates were 20, 40, 80, 120, 160, and 200 mV s^{-1}. The double-layer capacitance (C_{dl}) was estimated by the following equation:

$C_{dl} = (j_a - j_c)/(2 \cdot v) = (j_a + |j_c|)/(2 \cdot v) = \Delta j/(2 \cdot v),$

in which j_a and j_c are the anodic and cathodic voltammetric current density, respectively, recorded at the middle of the selected potential range (0.3 V vs. RHE), and v is the scan rate.

The ECSA values were calculated from the measured double-layer capacitance divided by the specific capacitance of an atomically smooth material ($C_{dl'}$, ~40 μF cm^{-2}): ECSA = C_{dl} / $C_{dl'} \times$ S, where S is the actual surface area of the electrode.[1]

5 cm^2 AEM electrolyzer cell measurements

A commercial AEM electrolyzer cell (active surface area of 5 cm^2) driven by Autolab PGSTAT302N (equipped with a 10A booster) was employed to examine the performance of the prepared electrodes. Square-shaped 5 cm^2 HNA-CA-H and HNA-CA-O as the cathode and anode were assembled

horizontally with Sustainion® X37-50 Grade RT Membrane as a separator in the commercial 5 cm^2 AEM electrolyzer cell. Nickel foams were used as gas diffusion layers (GDLs) on both sides of the cell. The cells were operated vertically, and 1 M KOH electrolytes were pumped into the cell with a flow rate of 200 ml min^{-1}. After 30 min of activation at a constant current density of 0.1 A cm^{-2}, the cells were characterized by recording I-U curves with a scan rate of 3 mV s^{-1} and the max current up to 5 A. As references, the other two cells with bare NP and HNA-CA as both the anode and cathode sides with Sustainion® X37-50 Grade RT Membrane as a separator are also tested in the same condition. Electrochemical Impedance Spectroscopy (EIS) was performed in galvanostatic mode with the workstation Autolab PGSTAT302N (equipped with a 10 A booster) in a frequency range from 0.1 Hz to 100 kHz. To analyze the EIS plots, the fitting procedure was performed using the equivalent circuit chosen based on the physical processes and their interactions in the system, which include ohmic, cathodic charge transfer (HER), anodic charge transfer (OER), and mass-transfer resistances. The fitting of the Nyquist plot is done by the commercially available ZView®.[2]

Table S1. HVOF spraying parameters.

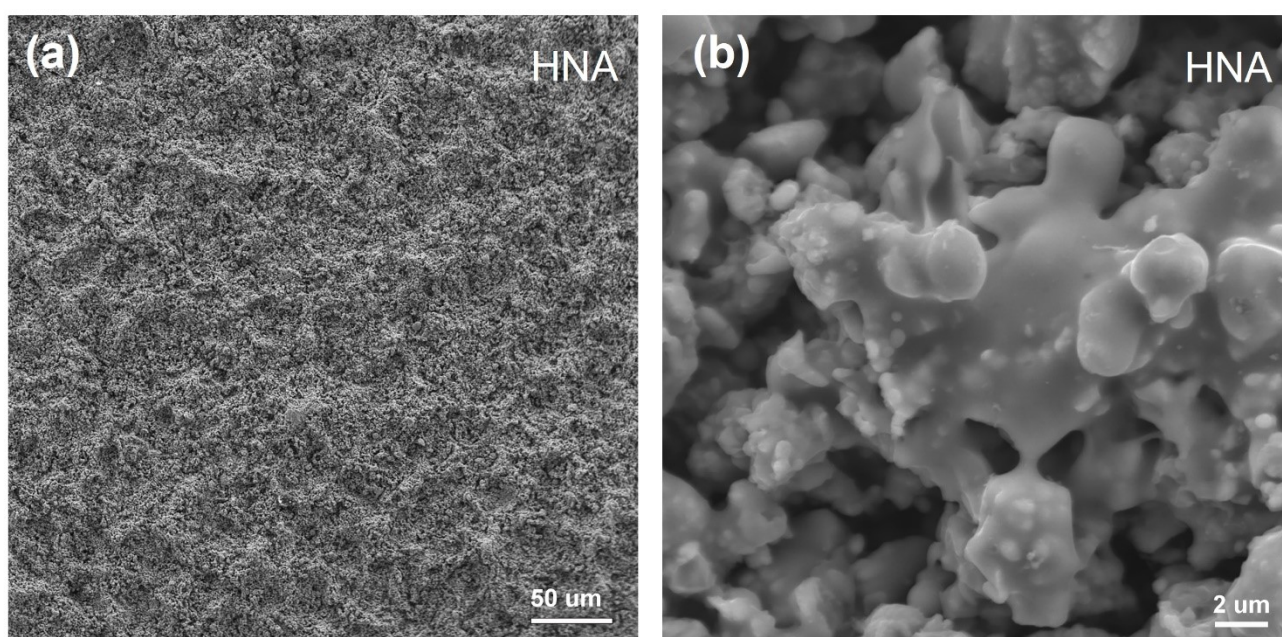| Parameters	Value
Torch	JP-5000
Oxidizer: Fuel	O_2 (1600L. min^{-1}); Kerosene (26 L. h^{-1})
Substrate	Nickel plate (NP)
Powder	Ni-Al (wt. %, 56-44) alloy
Powder flow	5 kg. h^{-1}
Projection distance	380 mm
External cooling	Three air jets

Figure S1. HNA coating. (a) SEM image, (b) HR-SEM image.

Table S2. SEM-EDS analysis of HNA, HNA-CA, HNA-CA-H, and HNA-CA-O.

Sample	Ni (wt. %)	Al (wt. %)	O (wt. %)
HNA	56.1	41.6	2.3
HNA-CA	76.6	13.9	9.5
HNA-CA-H	86.8	9.6	3.6
HNA-CA-O	79.6	8.1	12.3
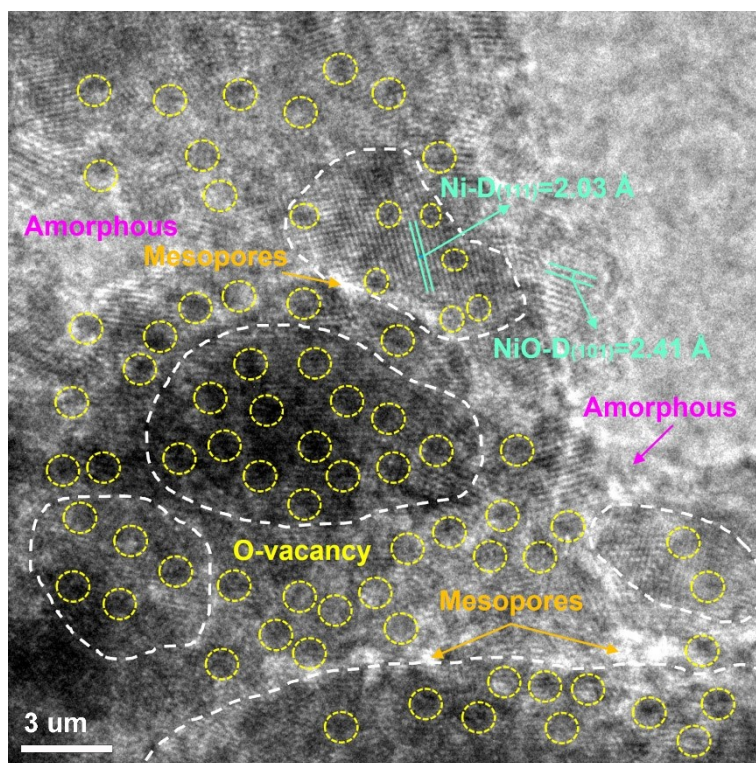
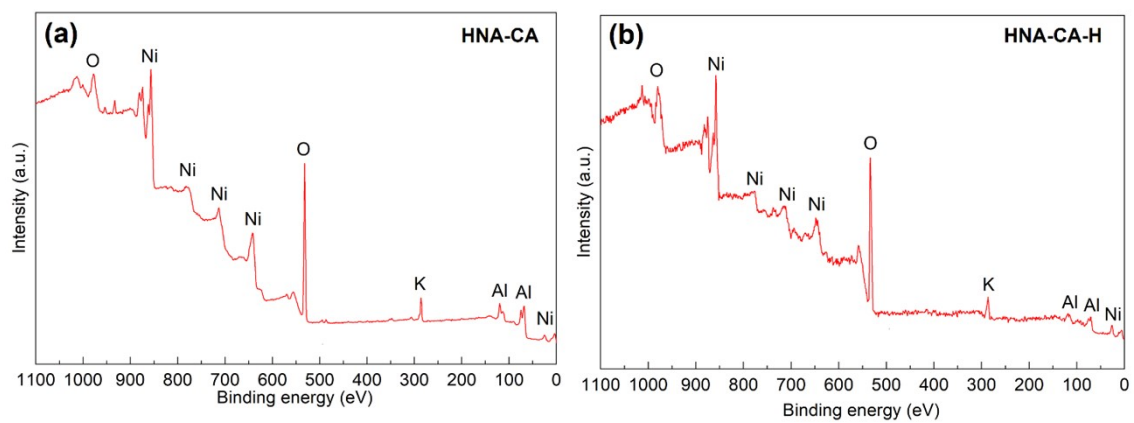Figure S2. HR-TEM image of the unique architecture of mesoporous Ni/NiO in the HNA-CA.

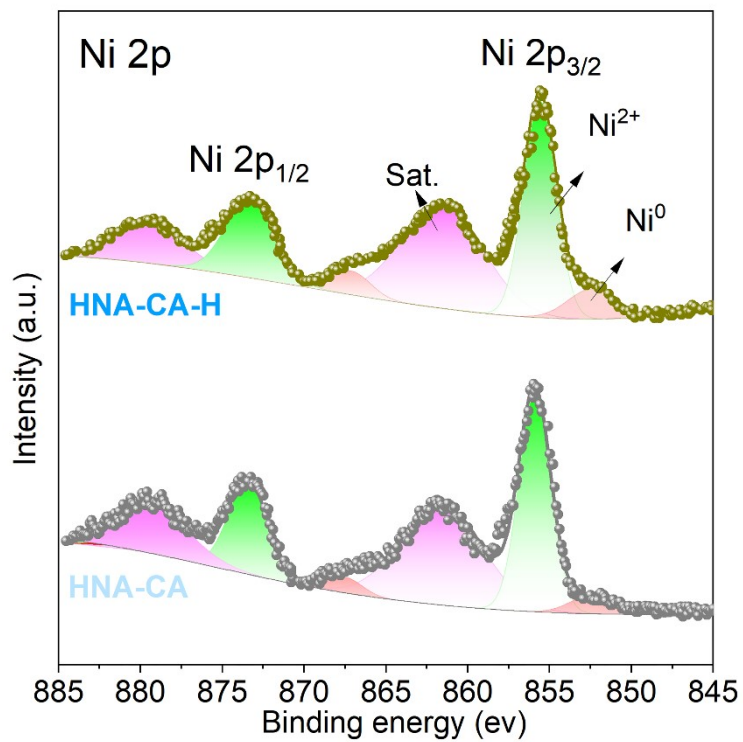Figure S3. XPS survey spectra. (a) HNA-CA; (c) HNA-CA-H.

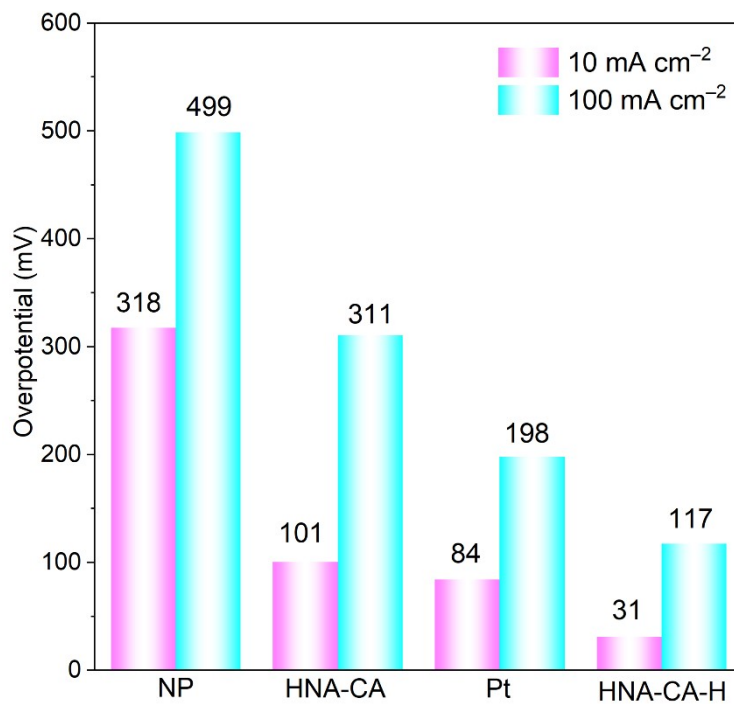Figure S4.The high-resolution XPS spectra of the HNA-CA, and HNA-CA-H catalysts: Ni 2p.

Figure S5. Overpotentials towards HER at the current density of –10 mA cm^{-2} and –100 mA cm^{-2} was illustrated and compared.

Table S3. The fitted equivalent circuit data (HER) of the employing samples.

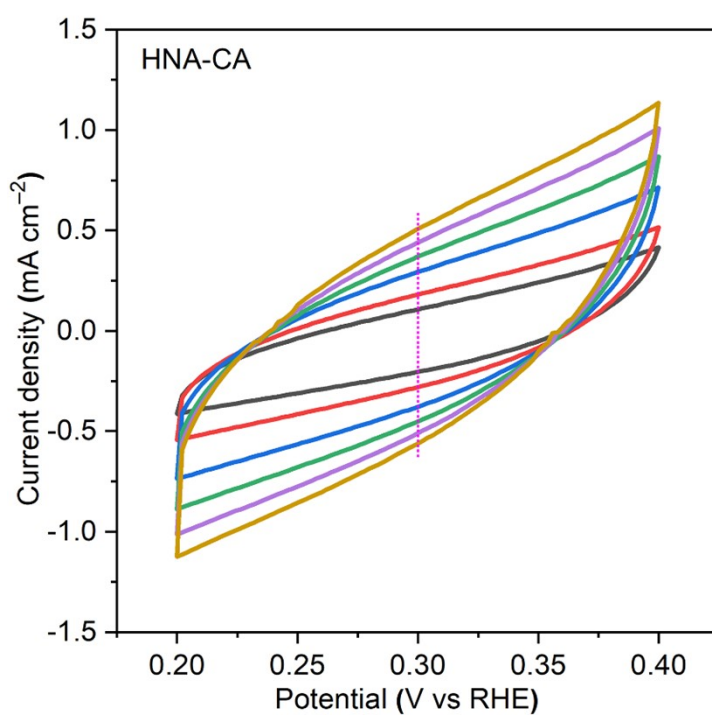| Samples	R_s / Ω cm^2	R_{ct} / Ω cm^2	CPE-T/S•s^(CPE-P)•cm^(–2)	CPE-P
Pt	0.87	1.52	3.52×10^{-2}	0.91
HNA-CA	0.89	2.93	2.41×10^{-2}	0.88
HNA-CA-H	0.89	0.64	3.10×10^{-2}	0.90
NP	0.88	10.89	3.08×10^{-2}	0.89

Figure S6. CV curves of HNA-CA at different scan rates. The potential window for CVs was 0.2–0.4 V vs. RHE. The scan rates were 20, 40, 80, 120, 160 and 200 mV s^{-1}. The double-layer capacitance (C_{dl}) was estimated by plotting the ΔJ = (Ja – Jc) at 0.3 V vs. RHE against the scan rate.
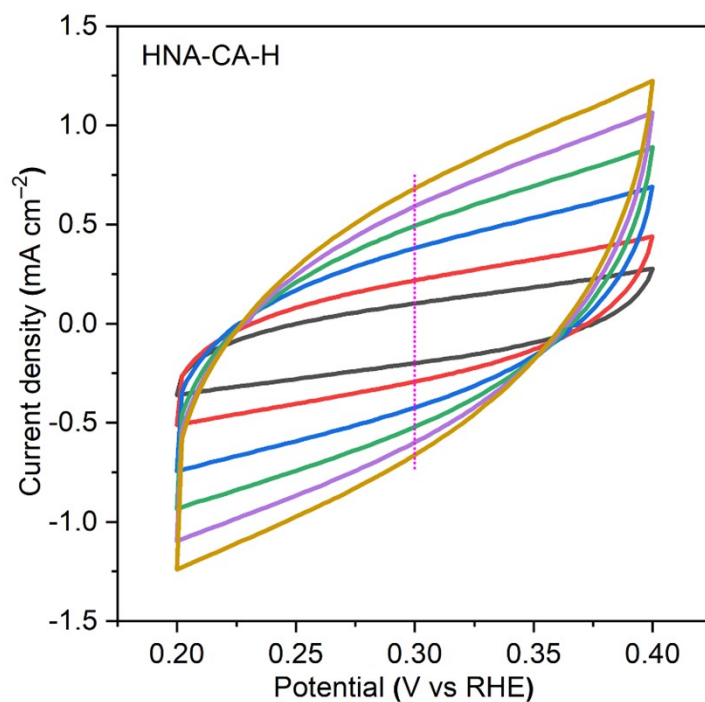
Figure S7. CV curves of HNA-CA-H at different scan rates. The potential window for CVs was 0.2–0.4 V vs. RHE. The scan rates were 20, 40, 80, 120, 160 and 200 mV s^{-1}. The double-layer capacitance (C_{dl}) was estimated by plotting the $\Delta J = (Ja - Jc)$ at 0.3 V vs. RHE against the scan rate.
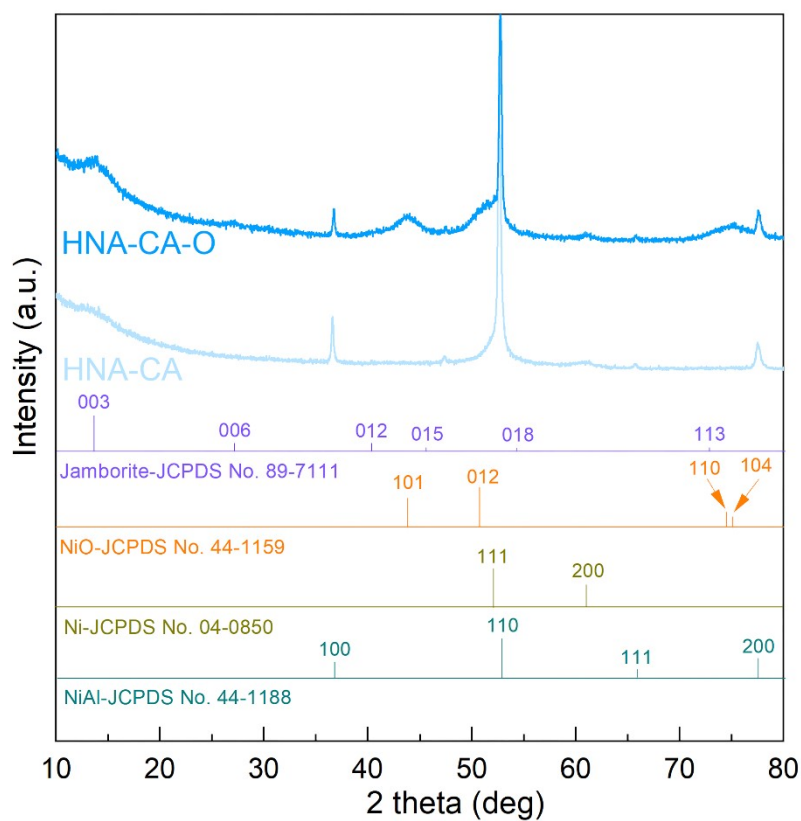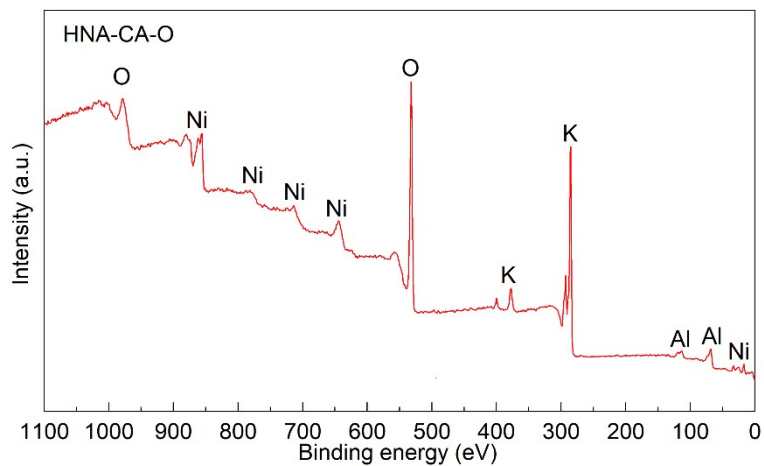

Figure S8. XRD patterns of the HNA-CA and HNA-CA-O.
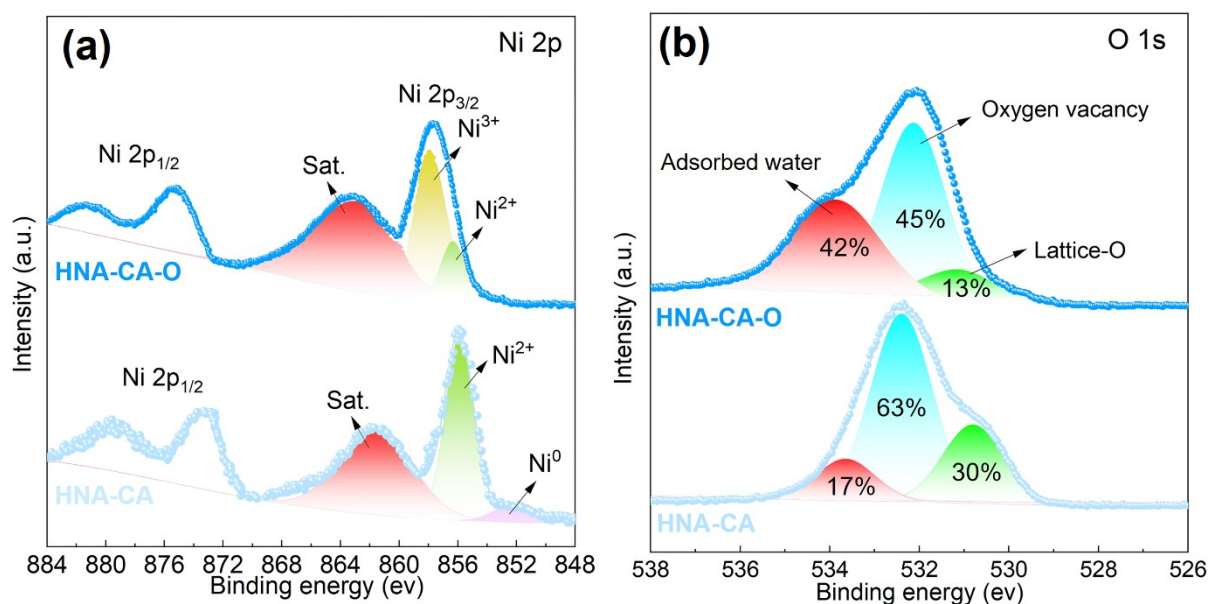
Figure S9. XPS survey spectra of HNA-CA-O.

Figure S10.The high-resolution XPS spectra of the HNA-CA, and HNA-CA-O catalysts: (a) Ni 2p; (b) O 1s.

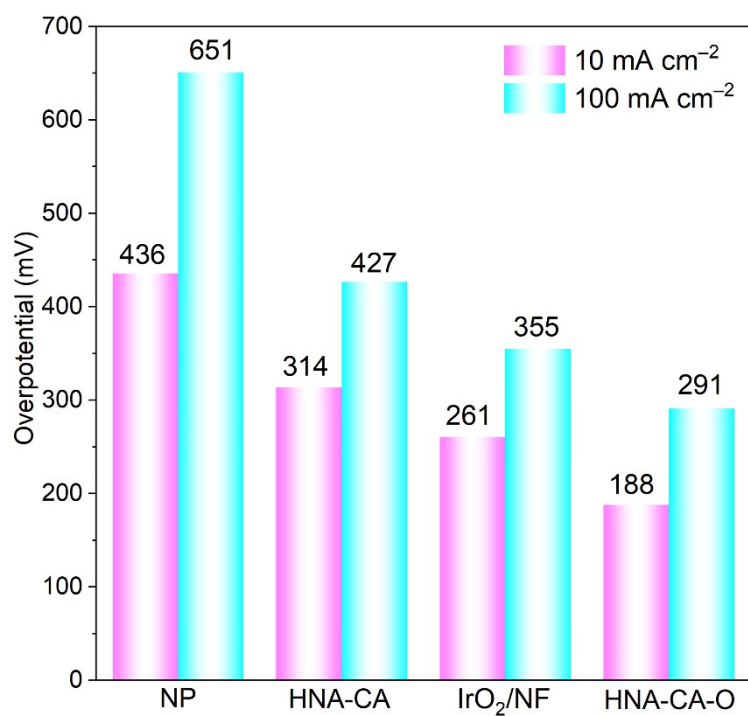Figure S11. Overpotentials towards OER at the current density of 10 mA cm^{-2} and 100 mA cm^{-2} was illustrated and compared.
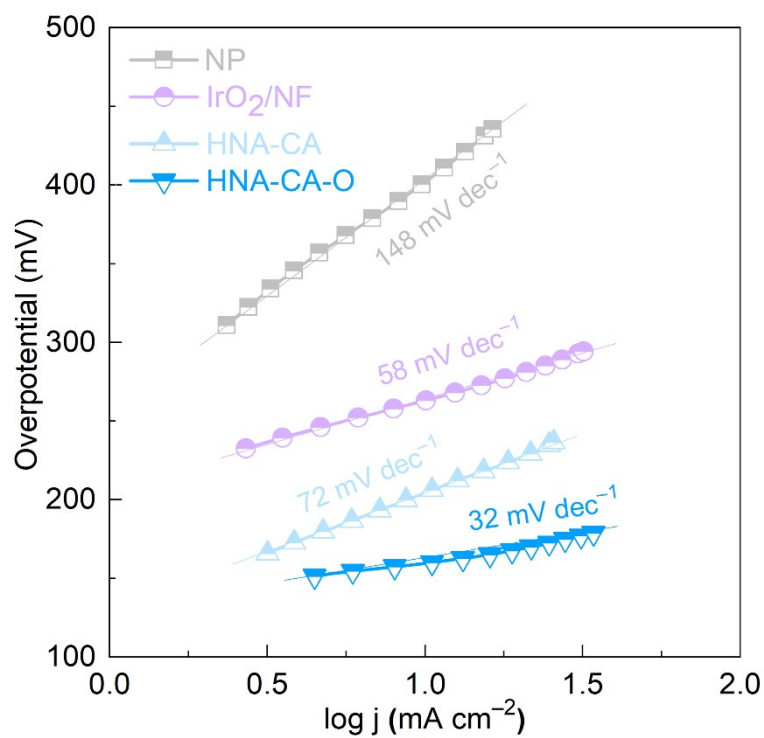

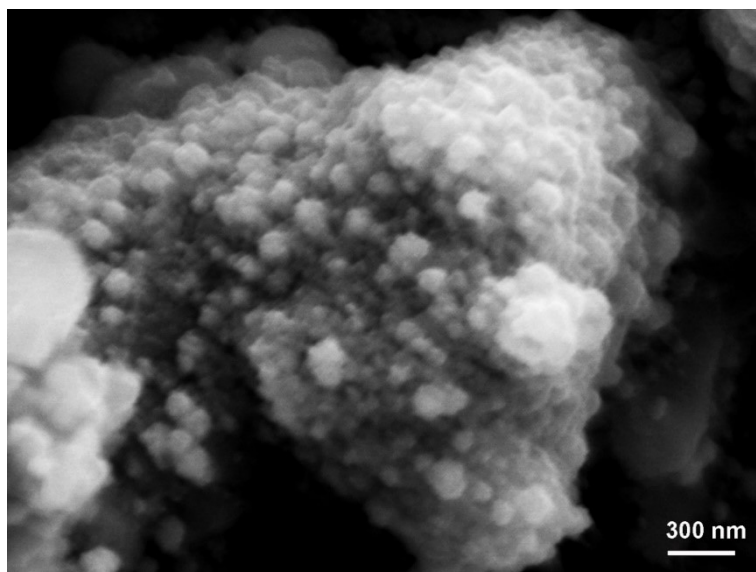Figure S12. Tafel plots of NP, IrO$_2$/NF, HNA-CA, and HNA-CA-O samples.

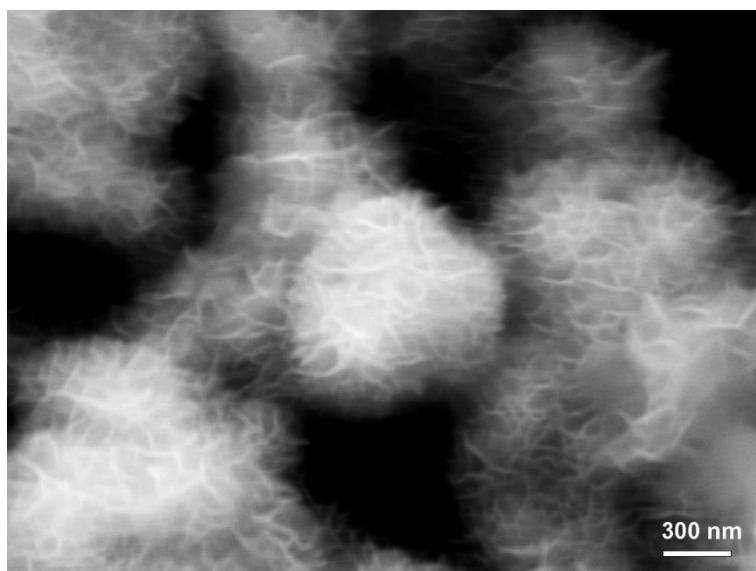Figure S13. SEM image of the HNA-CA-H electrode after durability test with 500 hours at 1 A cm^{-2}.

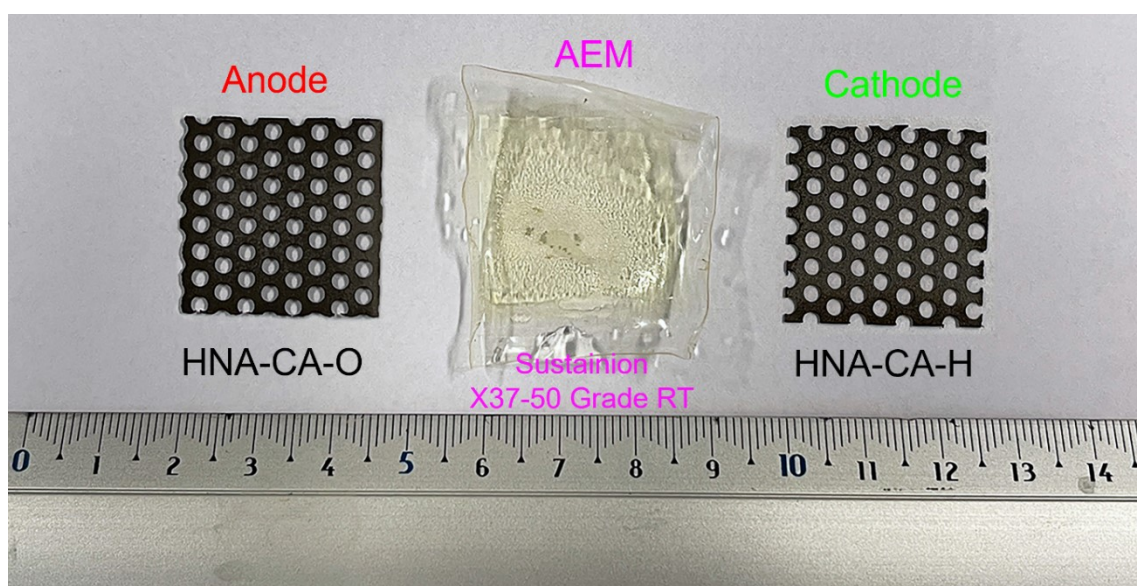Figure S14. SEM image of the HNA-CA-O electrode after durability test with 500 hours at 1 A cm^{-2}.

Figure S15. The optical image of the 5 cm^2 squared HNA-CA-H(–)‖HNA-CA-O(+) electrodes after 500 h durability test under 5 A (1 A cm^{-2}).

Table S4. The HER activity of the prepared catalysts compared with state-of-the-art HER catalysts reported.

Materials	Electrolyte	η_{10}, mV	η_{100}, mV	Tafel slope, mV/dec	Reference
HNA-CA-H	**1 M KOH**	**31**	**117**	**33**	**This work**
NiS-450	1 M KOH	115	300	65	Small Methods (2022) [3]
NiFeS@Ti$_3$C$_2$ MXene/NF	1 M KOH	150	450	177	Applied Catalysis B: Environmental (2023) [4]
Ni@C-N-AG	1 M KOH	150	350	68	Adv. Mater. Interfaces (2022) [5]
NCS-P	1 M KOH	77	275	68.5	Adv. Mater. Interfaces (2022) [6]
NiCoMnFe-P2	1 M KOH	200	310	104	Energy Fuels (2022) [7]
Ni$_2$Si PMEC	1 M KOH	80	261	55.5	Applied Catalysis B: Environmental (2024) [8]
Ni/NiFe$_2$O$_4$@PPy	1 M KOH	127	236	97	Chemical Engineering Journal (2023) [9]
Ni-Co-Fe-P NBs	1 M KOH	32	112	65	Applied Catalysis B: Environmental (2022) [10]
Ni$_{SA}$Fe$_{SA}$Ni$_{50}$Fe/CNT	1 M KOH	64	99	48.1	ACS Catal. 2022 [11]
NM@cNF/aNFO	1 M KOH	65	150	60	Chemical Engineering Journal (2022 [12]
Mo$_2$NiB$_2$	1 M KOH	160	250	71	Small (2022) [13]
NiFeCoS$_x$@FeNi$_3$	1 M KOH	88	200	116	J. Mater. Chem. A (2022) [14]
V-Ni$_3$FeN/Ni@N-GTs	1 M KOH	66	190	88	J. Mater. Chem. A (2022) [15]
m-NiTPyP/CNTs	1 M KOH	138	270	83	Adv. Mater. (2023) [16]
S-Fe-Ni/NF	1 M KOH	25	89	41	J. Mater. Chem. A (2023) [17]
Ni$_3$N/Ru/NCAC	1 M KOH	42	121	59	J. Mater. Chem. A (2023) [18]

Table S5.The OER activity of the prepared catalysts compared with state-of-the-art OER catalysts reported.

Materials	Electrolyte	η_{10}, mV	η_{100}, mV	Tafel slope, mV/dec	Reference
HNA-CA-H	**1 M KOH**	**188**	**291**	**32**	**This work**
NiS-450	1 M KOH	172	360	65	Small Methods (2022) [3]
NiFeS@Ti$_3$C$_2$ MXene/NF	1 M KOH	270	360	45	Applied Catalysis B: Environmental (2023) [4]
Ni@C-N-AG	1 M KOH	290	490	93	Adv. Mater. Interfaces (2022) [5]
NCS-P	1 M KOH	273	355	42.2	Adv. Mater. Interfaces (2022) [6]
NiCoMnFe	1 M KOH	286	340	53	Energy Fuels (2022) [7]
Ni$_2$Si PMEC	1 M KOH	273	353	72.4	Applied Catalysis B: Environmental (2024) [8]
Ni/NiFe$_2$O$_4$@PPy	1 M KOH	265	370	99	Chemical Engineering Journal (2023) [9]
Ni-Co-Fe-P NBs	1 M KOH	187	221	29	Applied Catalysis B: Environmental (2022) [10]
Ni$_{SA}$Fe$_{SA}$Ni$_{50}$Fe/CNT	1 M KOH	227	270	41.8	ACS Catal. 2022 [11]
NM@cNF/aNFO	1 M KOH	100	182	19	Chemical Engineering Journal (2022) [12]
Mo$_2$NiB$_2$	1 M KOH	280	NA	57	Small (2022) [13]
NiFeCoS$_x$@FeNi$_3$	1 M KOH	210	230	45	J. Mater. Chem. A (2022) [14]
V-Ni$_3$FeN/Ni@N-GTs	1 M KOH	252	300	29	J. Mater. Chem. A (2022) [15]
NiFeMOFs	1 M KOH	258	NA	49	Adv. Energy Mater., 2021 [19]
Ni (S-Fe-Ni)	1 M KOH	200	235	31.4	J. Mater. Chem. A (2023) [17]
m-NiTPyP/CNTs	1 M KOH	267	320	33.1	Adv. Mater. (2023) [16]
Ni$_3$N/Ru/NCAC	0.1 M KOH	288	NA	60	J. Mater. Chem. A (2023) [18]

References

1. C. Liang, P. Zou, A. Nairan, Y. Zhang, J. Liu, K. Liu, ... &   and C. Yang, *Energy Environ. Sci.*, 2020, **13**, 86-95.

2. D. J. S. A. Johnson, Inc, 2000.

3. G. Bahuguna, A. Cohen, N. Harpak, B. Filanovsky and F. Patolsky, *Small Methods*, 2022, **6**, e2200181.

4. D. Chanda, K. Kannan, J. Gautam, M. M. Meshesha, S. G. Jang, V. A. Dinh and B. L. Yang, *Applied Catalysis B: Environmental*, 2023, **321**.

5. S. Chen, X. Min, Y. Zhao, X. Wu, D. Zhang, X. Hou, X. Wu, Y. g. Liu, Z. Huang, A. M. Abdelkader, K. Xi and M. Fang, *Advanced Materials Interfaces*, 2022, **9**.

6. S. Garain, C. Dang Van, S. Choi, T. Nguyen Dang, J. W. Ager, K. T. Nam, H. Shin and M. H. Lee, *Advanced Materials Interfaces*, 2022, **9**.

7. M. M. Hasan, A. K. Gomaa, G. E. Khedr, K. E. Salem, B. S. Shaheen and N. K. Allam, *Energy & Fuels*, 2022, **36**, 14371-14381.

8. Z. He, Y. He, Y. Qiu, Q. Zhao, Z. Wang, X. Kang, L. Yu, L. Wu and Y. Jiang, *Applied Catalysis B: Environmental*, 2024, **342**.

9. L. Jia, G. Du, D. Han, Y. Wang, W. Zhao, Q. Su, S. Ding and B. Xu, *Chem. Eng. J.*, 2023, **454**.

10. A. Li, L. Zhang, F. Wang, L. Zhang, L. Li, H. Chen and Z. Wei, *Applied Catalysis B: Environmental*, 2022, **310**.

11. W. Luo, Y. Wang, L. Luo, S. Gong, M. Wei, Y. Li, X. Gan, Y. Zhao, Z. Zhu and Z. Li, *ACS Catalysis*, 2022, **12**,

1167-1179.

12. Q. lv, B. Yao, W. Zhang, L. She, W. Ren, L. Hou, Y. Fautrelle, X. Lu, X. Yu and X. Li, *Chem. Eng. J.*, 2022, **446**.

13. A. Saad, Y. Gao, K. A. Owusu, W. Liu, Y. Wu, A. Ramiere, H. Guo, P. Tsiakaras and X. Cai, *Small*, 2022, **18**, e2104303.

14. J. Shen, Q. Li, W. Zhang, Z. Cai, L. Cui, X. Liu and J. Liu, *J. Mater. Chem. A*, 2022, **10**, 5442-5451.

15. G. Song, S. Luo, Q. Zhou, J. Zou, Y. Lin, L. Wang, G. Li, A. Meng and Z. Li, *J. Mater. Chem. A*, 2022, **10**, 18877-18888.

16. Y. Zhang, S. Chen, Y. Zhang, R. Li, B. Zhao and T. Peng, *Adv. Mater.*, 2023, **35**, e2210727.

17. Z. Zang, Q. Guo, X. Li, Y. Cheng, L. Li, X. Yu, Z. Lu, X. Yang, X. Zhang and H. Liu, *J. Mater. Chem. A*, 2023, **11**, 4661-4671.

18. X. Zhao, X. Yong, Q. Ji, Z. Yang, Y. Song, Y. Sun, Z. Cai, J. Xu, L. Li, S. Shi, F. Chen, C. Li, P. Wang and J.-B. Baek, *J. Mater. Chem. A*, 2023, **11**, 12726-12734.

19. Y. Wang, B. Liu, X. Shen, H. Arandiyan, T. Zhao, Y. Li and C. Zhao, *Adv. Energy Mater.*, 2021, **11**, 2003759.